PREDICTING HUMAN GEOMETRY-RELATED FACTORS FOR DETAILED RADIATION ANALYSIS IN INDOOR SPACES

K. Kubaha, D. Fiala and K. J. Lomas
Institute of Energy and Sustainable Development (IESD), De Montfort University,
Scraptoft Campus, Leicester, UK

ABSTRACT

In this study, formulae for predicting projected area factors and view factors of individual body parts of standing and sedentary humans for detailed radiation analysis were developed. For this purpose, detailed geometry models of the human body were generated representing an average subject with a height of 1.75 m and a DuBois' area of 1.83 m^2. Thermal analysis software incorporating advanced, voxel-based ray tracing techniques and regression analysis were deployed to model the local projected area factors of humans exposed to direct and diffuse solar radiation. A method was developed to predict view factors of individual body parts based on the projected area factor calculations. This technique makes it possible to predict view factors between individual body parts and surrounding surfaces for almost any arbitrary geometrical configurations of the radiation envelope. The predicted view factors were validated and showed good agreement with experimental data available in the literature.

INTRODUCTION

Radiative heat exchange between the human body and the environment plays an important role in the human heat transfer and thermal comfort. In buildings, humans are frequently exposed to inhomogeneous radiation that causes occupants discomfort e.g. in close proximity of cold windows, hot radiators, etc. Moreover, asymmetric radiation due to non-uniform surface temperatures, direct solar radiation or other high intensity artificial sources causes local discomfort at individual body parts and makes occupied zones uncomfortable. Thermal discomfort causes restrictions in the usability and functionality of spaces, and reduces occupants' performance at the workplace. The ability to predict the inhomogeneous human radiative heat exchange also has benefits for assessing work efficiency, safety and health.

Two different geometry factors are needed to predict the human radiative heat exchange. Projected area factors (f_p) are needed to predict the short-wave radiation, while view factors (φ) between the human body and surfaces of the enclosure are required when predicting the long-wave radiative heat exchange between humans and their surroundings. Both factors have been subjected to various experimental investigations in literature but the results are available only for the whole body. They are not available for individual body parts required for detailed human radiation analysis.

Fortunately, in recent years, sophisticated computer simulation software and thermal analysis tools have emerged which make detailed modelling and prediction of the human radiative heat exchange in buildings possible e.g. RadTherm (RadTherm, 2001), Poser4 (Poser4, 2000), ESP-r (Clark and McLean, 1988), and diverse CFD package (CFX-5, 2002). Such software is capable of dealing with highly complex geometries such as the human body (Figure 1) and predictions compare well with experimental measurements, Curran A.R. et al. (1995), Lomas et al. (1994) and Cook, M. J. and Lomas K. J. (1998). Furthermore multi-node models of the human thermal system e.g. Stolwijk (1970) and Fiala (1999, 2001) have been developed as there is a growing need to predict human physiological and thermal comfort responses in various disciplines of science and technology. Also these models have been shown to reproduce well with in experimental results, Fiala (2001, 2003).

The aim of this study is to develop formulae and techniques for calculating human projected area factors and view factors for individual body parts of the human body. The new formulae and calculation techniques developed in this study can be used in conjunction e.g. with multi-segmental models of the human temperature regulation and thermal comfort. As an exampale the IESD-Fiala multi-segmental dynamic model was used to incorporate the formulae and techniques to predict human responses to thermally asymmetric environments. The simulation results are compared with experimental data in this paper.

METHODOLOGY

Human body models

The human body, both standing and sedentary, was modelled as having left-right symmetry and a stress-free position using the Poser4 software (Poser4,

2000). The software is capable of generating detailed 3D models of the human body at almost any arbitrary posture. The models consisted of 10995 small surface

Table 1. Area of individual body parts of the human body model.

| No.	Body parts	Body sectors	Surface Area [m^2]
1	Head	Head	0.0525
		Forehead	0.0050
2	Face	Anterior	0.0193
		Left & right	0.0110
3	Neck	Anterior	0.0050
		L.& R. Exterior	0.0094
		Posterior	0.0068
4	Shoulder	Left	0.0205
		Right	0.0205
5	Thorax	Anterior	0.1115
		L. & R. Inferior	0.0093
		Posterior	0.0916
6	Abdomen	Anterior	0.1104
		L. & R. Inferior	0.0401
		Posterior	0.1091
7	Upper arms	Anterior	0.0144
		Exterior	0.0292
		Inferior	0.0098
		Posterior	0.0143
8	Lower arms	Anterior	0.0092
		Exterior	0.0269
		Inferior	0.0268
		Posterior	0.0124
9	Hands	Handback	0.0285
		Palm	0.0276
10	Upper legs	Anterior	0.0466
		Exterior	0.0503
		Inferior	0.0407
		Posterior	0.0386
11	Lower legs	Anterior	0.0254
		Exterior	0.0390
		Inferior	0.0335
		Posterior	0.0372
12	Feet	Instep	0.0400
		Sole	0.0203
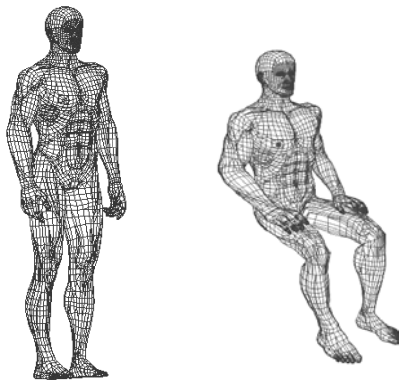
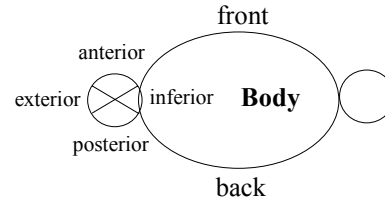**Figure 1**. *The human body geometry models used in the study*.

Figure 2. *Subdivision of body parts into spatial sectors.*

elements to provide sufficient detail for the radiation simulations (Figure 1). The elements were grouped together into 59 main body parts (Table 1) and spatial sectors (Figure 2) representing an average male with a height of 1.75m and a DuBois' area of 1.83 m^2.

Simulation strategy

The humanoid geometries were imported into the thermal analysis software package (RadTherm, 2001) which uses a voxel-based ray tracing technique to predict the absorbed short-wave radiation energy at each of the 10995 surface elements. At this stage the surface elements were defined as black body radiators with an absorptivity of one. Given the incident flux, the absorbed radiation of each surface element was calculated by the software. The results were then postprocessed integrating the elemental fluxes to obtain projected area factors for individual body sectors (face, forehead etc.).

The total amount of solar radiation absorbed by a body sector consisting of n surface elements was obtained as the sum of predicted nodal quantities, $Q_{a,i}$. For a group of body nodes, the projected area factor, f_p, is thus presented as:

$$f_p = \frac{1}{q_s} \times \frac{\sum_{i=1}^{n} Q_{a,i}}{\sum_{i=1}^{n} A_i} \qquad (1)$$

where f_p = projected area factor of a body
              sector;   [-]
     $Q_{a,i}$ = solar radiation absorbed by
              surface element, i;   [W]
     q_s = incident solar radiation flux;   [W/m^2]
     A_i = area of surface element, i.   [m^2]

Modelling projected area factors

The projected area factors were modelled for both direct and diffuse short-wave radiation. They were considered as a function of the azimuth angle, α, and altitude angle, β, for the case of direct short-wave radiation. The angles were included for all spherical positions of the sun, hence, α varied from 0 to 360° (due north, clockwise) and β varied from –90° to 90°. For the diffuse short-wave radiation case the projected area factors were considered as a function

of the ground reflectance, ρ, which was varied between 0 and 1 while assuming an isotropic sky.

Simple and polynomial regressions were used to derive the coefficients of the projected area factor equations. If any regression coefficient was not significantly different from zero at the 0.95 confidence level, a new regression was run without the non-significant variable. The two-tailed population t-test was applied to determine the significance level of the regression coefficients.

For direct short-wave radiation and most body sectors (such as anterior, posterior and some exterior body sectors) the projected area factor curves could be described as periodic *cosine* functions of the azimuth angle, α. However, the functions were not reproduced well for some body sectors that were 'hidden' or 'shaded' by other body parts such as the inferior body sectors. For these, it was necessary to account for the shading effect by deriving a so called 'shading-function' as a part of the final solution for each body sector:

$$f_p = \Omega \times S \qquad (2)$$

where $\qquad \Omega = A\cos(c_1\alpha + c_0) + B \qquad (3)$

and $S = 1 + \dfrac{\tanh(d_1\alpha + d_0)}{2} + \dfrac{\tanh(e_1\alpha + e_0)}{2}. \quad (4)$

In equation (2), Ω is the basic function and S is the shading function of a body sector. The coefficients A, B, d_1, d_0 and e_1, e_0 as well as c_0 and c_1 were determined by regression analysis. Each of these coefficients were functions of the altitude angle, β. The regression coefficients A, B, d_1, d_0, e_1 and e_0 were determined using polynomials of up to order four, while c_0 and c_1 were considered as coefficients of linear functions of β.

The projected area factors for diffuse short-wave radiation of individual body sectors were modelled as linear functions of the ground reflectance:

$$f_p = c_1\rho + c_0 \qquad (5)$$

where $\quad f_p \quad = \quad$ projected area factor of a body

sector; [-]
$\rho \quad = \quad$ ground reflectance; [-]
c_0 and $c_1 \quad = \quad$ regression coefficients of a body sector. [-]

Modelling view factors

For each surface sector of the human body, A_b, and any arbitrary plane of the radiation enclosure, A_w, the view factor is a function of their relative geometric relationships:

$$\varphi_{b,w} = \frac{1}{\pi A_b} \iint\limits_{A_b A_w} \frac{\cos\beta_b \cos\beta_w}{r^2} dA_b dA_w. \quad (6)$$

Note that the term $cos\beta_b dA_b$ is the (differential) projected area (dA_p) of the body sector, A_b. The corresponding projected area factor (df_p) is then the ratio of dA_p and the corresponding actual area. Equation (6) can therefore be expressed as a function of the projected area factor, f_p, which, when recast in numerical integration form, gives:

$$\varphi_{b,w} = \frac{1}{\pi A_b} \sum_{j=1}^{n} \sum_{i=1}^{m} \frac{1}{r_{j,i}^2} \times f_{p_{j,i}} \Delta A_{b_j} \times \cos\beta_{w_{j,i}} \Delta A_{wi} \quad (7)$$

where

$\varphi_{b,w} \quad = \quad$ view factor of the body sector, A_b, with respect to plane, A_w; [-]
$j \quad = \quad$ running number for surface elements of the body sector A_b; [-]
$i \quad = \quad$ running number for plane elements of the plane A_w; [-]
$r_{j,i}^2 \quad = \quad$ square absolute of the distance vector $\bar{r}$ between the body element, j and the plane element, i; [m]
$f_{p_{j,i}} \quad = \quad$ projected area factor of body surface, j, with respect to plane element, i; [-]
$\beta_{w_{j,i}} \quad = \quad$ angle between $\bar{r}$ and the vector normal to the plane element, i; [rad]
$A_{wi} \quad = \quad$ area of the plane element, i; [m²]
$A_{bj} \quad = \quad$ area of the body surface element, j; [m²]
$A_b \quad = \quad$ total area of the body sector. [m²]

Introducing the projected area factors, f_p, for a whole body sector (equation 1), assuming the central coordinate (x_b, y_b, z_b) is its representative coordinate, and the central coordinate (x_{wi}, y_{wi}, z_{wi}) is the representative coordinate of the plane element i, (Figure 3), then the view factor of the body sector with respect to the plane is

$$\varphi_{b,w} = \frac{1}{\pi} \sum_{i=1}^{m} \frac{1}{r_i^2} \times f_{pi} \times \cos\beta_{wi} \Delta A_{wi} \qquad (8)$$

where $\quad f_{pi} \quad = \quad$ projected area factor of the body sector, A_b, with respect to the plane element, A_{wi}; [-]
$m \quad = \quad$ number of surface elements of the plane, A_w. [-]
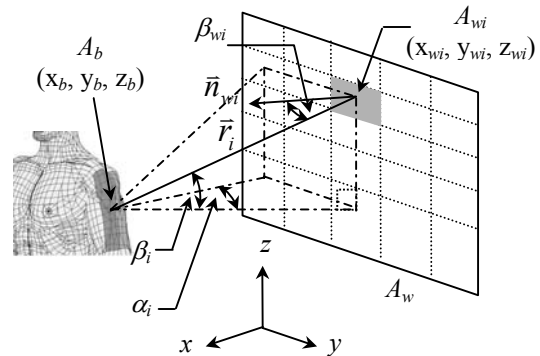

Figure 3. *Geometric data involved in the calculation of the view factor between a body sector and a plane.*

The term f_{pi} in equation (8) depends on the azimuth angle, α_i, and the altitude angle, β_i, according to equations (2) to (4). Here α_i and β_i between the body sector and a surface element of the wall is calculated by using the following equations:

$$\tan(\alpha_i) = \frac{(y_b - y_{wi})}{(x_b - x_{wi})} \qquad (9)$$

which gives $\quad \alpha_i = \tan^{-1}\left\{\frac{(y_b - y_{wi})}{(x_b - x_{wi})}\right\} \qquad (10)$

and

$$\tan(\beta_i) = \frac{(z_{wi} - z_b)}{\sqrt{(x_b - x_{wi})^2 + (y_b - y_{wi})^2 + (z_b - z_{wi})^2}} \qquad (11)$$

hence

$$\beta_i = \tan^{-1}\left\{\frac{(z_{wi} - z_{bi})}{\sqrt{(x_b - x_{wi})^2 + (y_b - y_{wi})^2 + (z_b - z_{wi})^2}}\right\}. \qquad (12)$$

The angle, β_{wi}, between $\vec{r}_i$ and the normal vector, $\vec{n}_{wi}$, of the plane element, i, is determined by:

$$\cos\beta_{wi} = \frac{\vec{n}_{wi} \cdot \vec{r}_i}{|\vec{r}_i|} \qquad (13)$$

where $\vec{n}_{wi}$ = normal vector of the plane element, i

$$\vec{n}_{wi} = \begin{bmatrix} n_{xi} \\ n_{yi} \\ n_{zi} \end{bmatrix}; \ n_{xi} = \begin{bmatrix} 1 \\ 0 \\ 0 \end{bmatrix}; \ n_{yi} = \begin{bmatrix} 0 \\ 1 \\ 0 \end{bmatrix}; \ n_{zi} = \begin{bmatrix} 0 \\ 0 \\ 1 \end{bmatrix} \qquad (14)$$

$$\vec{r}_i = \begin{bmatrix} r_{xi} \\ r_{yi} \\ r_{zi} \end{bmatrix} = \begin{bmatrix} x_b - x_{wi} \\ y_b - y_{wi} \\ z_b - z_{wi} \end{bmatrix} \qquad (15)$$

and $\qquad |\vec{r}_i| = \sqrt{r_{xi}^2 + r_{yi}^2 + r_{zi}^2}. \qquad (16)$

RESULTS AND DISCUSSION

Verification

For verification purposes, the prediction of projected area factors and view factors for each individual body sector of the standing and sedentary human, were initially compared with the results obtained by the voxel-based ray tracing technique, (RadTherm, 2001).

As examples, the projected area factors of the right face exterior and forehead of a standing and sedentary person are illustrated, for direct short-wave radiation in Figure 4, and for diffuse short-wave radiation in Figure 5.
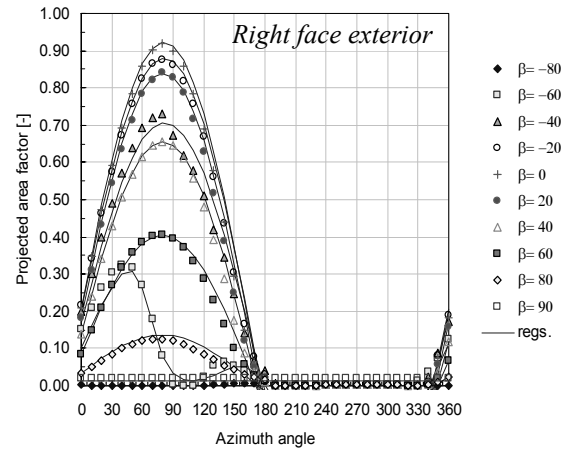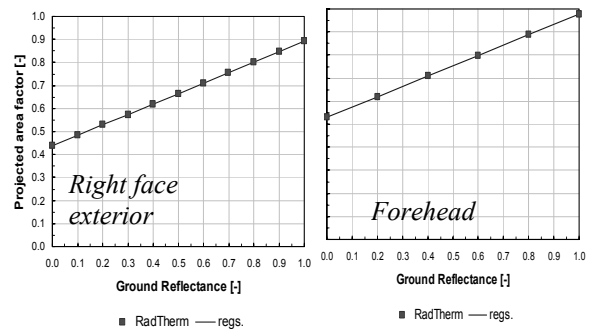

a) Standing posture
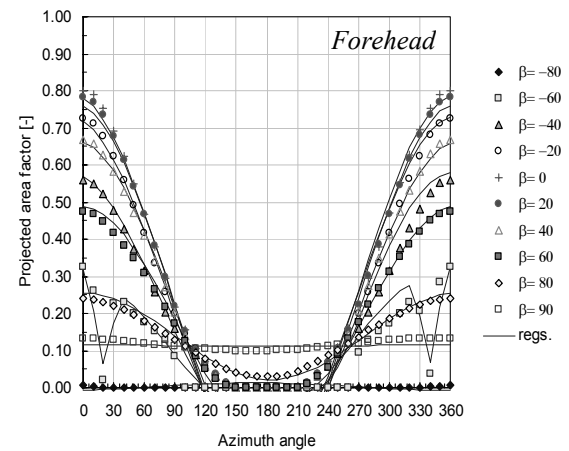
b) Sedentary posture

Figure 4. *Projected area factor curves for direct short-wave radiation of two body sectors.*

The predictions from the regression equations (solid lines) are in good agreement with the predictions (data points) across the complete range of azimuth (α) and altitude (β) angles. As can be seen, also the shading function accounted appropriately for the shadowing effects by other body parts (e.g. at $\beta = -60°$, between $40°<\alpha<160°$ for right face exterior and at $\beta = -60°$, between $10°<\alpha<40°$ and $320°<\alpha<350°$ for forehead, Figure 4).

a) Standing posture   b) Sedentary posture

Figure 5. *Projected area factor curves for diffuse short-wave radiation of two body sectors.*

For diffuse short-wave radiation (Figure 5) the regression equations provided a very good fit to the f_p-factors for all body sectors and clearly performed as linear equation with correlation coefficients close to unity.

As an example, the view factors of the left arm (lower exterior part) and anterior thorax with respect to a front wall for both standing and sedentary postures are shown in Figure 6. Solid lines represent predicted view factors using equation (8), the data points represent the results obtained by the voxel-based ray tracing technique. The predictions and the simulated results were compared by varying the dimensionless values a/c and b/c between 0.2 and 10 (see Figure 7 for geometric configuration). As can be seen, the predictions were in good agreement with the RadTherm values.
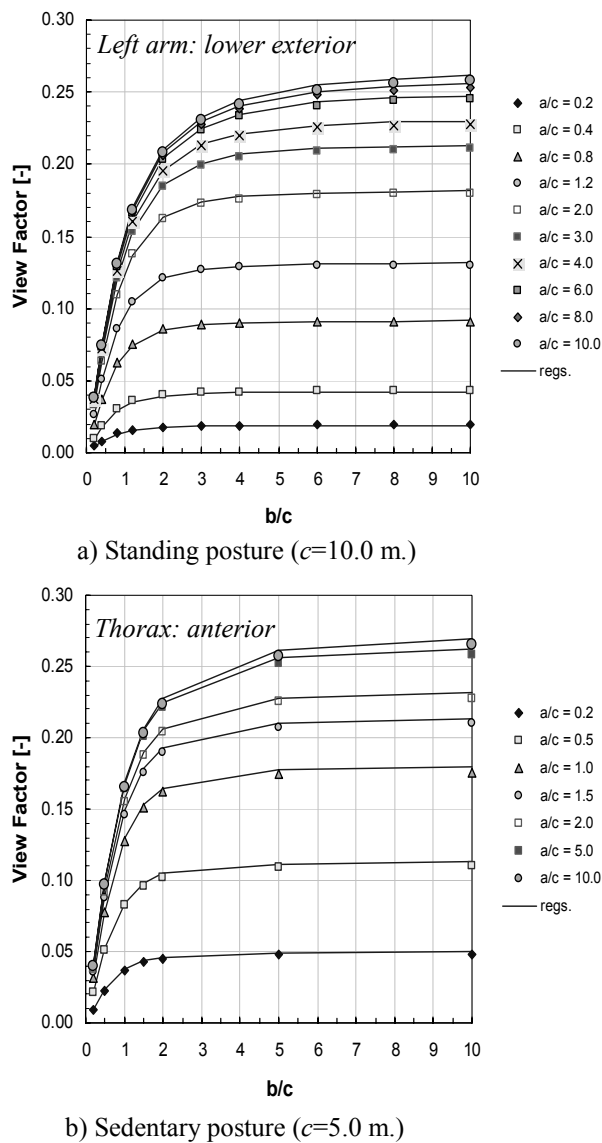
Validation

To date, most experimental data is available just for the whole body. Therefore, the predicted results obtained for individual body sectors were integrated over the whole body and were compared with experimental results provided by Fanger (1970) and Horikoshi et al. (1996).

Thereby, the view factors of individual body sectors were predicted with respect to four geometric configurations: front wall (FW), sidewall (SW), ceiling (CE), and floor (FL), Figure 7. For validation purposes the geometry was set up to match the experiments of Fanger in this study. The results described in this paper are however equally valid for any arbitrary enclosure.
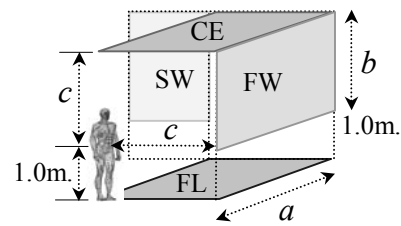

Figure 7. *Geometric configuration of the enclosure used in the validation work.*

The view factors were calculated by varying the dimensionless distances a/c and b/c. Here, a and b are the length and height of a plane and c is distance between the centre of the body and the plane.
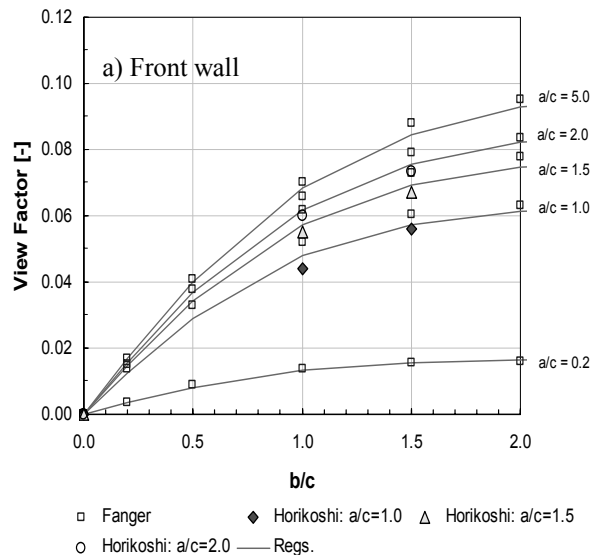

a) Standing posture (c=10.0 m.)

b) Sedentary posture (c=5.0 m.)

Figure 6. *View factors between body sectors and a wall in front of a person.*

Figure 8. *View factors between the whole body and planes in front of a standing person.*

b) Sidewall

Fanger   ◆ Horikoshi: a/c=1.0   △ Horikoshi: a/c=1.5
○ Horikoshi: a/c=2.0   —— Regs.

c) Ceiling

Fanger   ◆ Horikoshi: a/c = 1.0   —— Regs.

d) Floor

Fanger   ◆ Horikoshi: a/c =1.0   △ Horikoshi: a/c =1.5
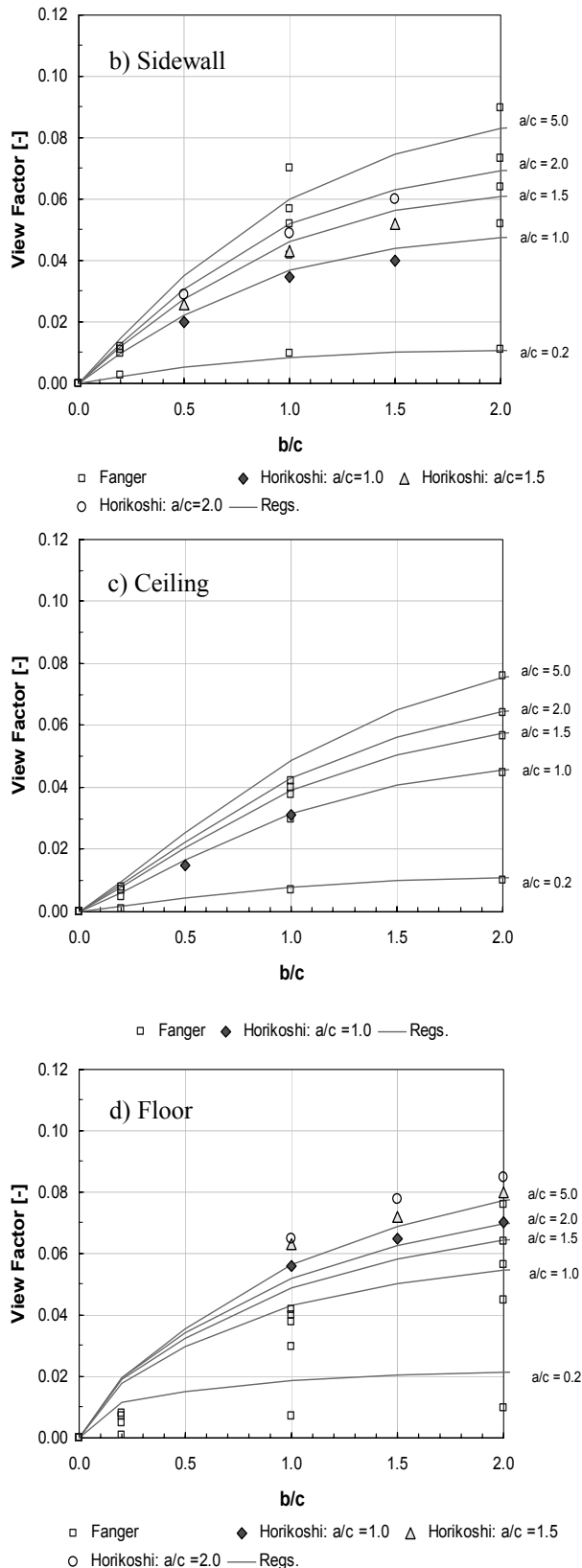○ Horikoshi: a/c =2.0   —— Regs.

Figure 8. (Continued).

The predictions were performed by setting *a/c* and *b/c* at 0.2, 1.0, 1.5, 2.0 and 5.0. The distance, *c*, between the body and the walls (front wall and sidewall) was set at 1.0 m and the ceiling above the floor was 3.0 m. It can be seen that there is a good agreement between the predictions (solid lines) and experimental values for most *a/c* and *b/c* values. An exception form predicted view factors to the floor which are greater than in the experiments of Fanger but lower than the experimental results of Horikoshi.

Some reasons for the discrepancies between predictions and measurements are: a. the human body simulated could differ in geometry from the subjects in the experiments and b. there would be differences between postures simulated and the standing and sedentary postures adopted by experimental subjects. Further comparisons of view factors for the sedentary posture are shown in the Appendix.

As a final experimental validation, and to illustrate the value of the link between the multi-node dynamic IESD-Fiala comfort model and the radiation model, the skin temperatures, rectal temperature and sweating rates were predicted in extremely asymmetric radiant environments. The results were compared against experimental data obtained by Hall and Klemm (1969).

In the experiments the human body was laid down supine on a net in the centre of a chamber which was divided into an upper and lower section. Five experiments were conducted with the wall temperatures of the upper half and the lower half set at 104˚C and –6.7˚C, 93˚C and –6.7˚C, 82˚C and –6.7˚C, 65˚C and –11.0˚C and 53˚C and –11.0˚C, respectively (experiment 1, 2, 3, 4 and 5). The air velocity, average air temperature and water vapour pressure in the chamber were 0.08 m/s, 20˚C and 2.5 mmHg, respectively. The subjects were clad only in underwear (I_{cl}=0.3 clo).
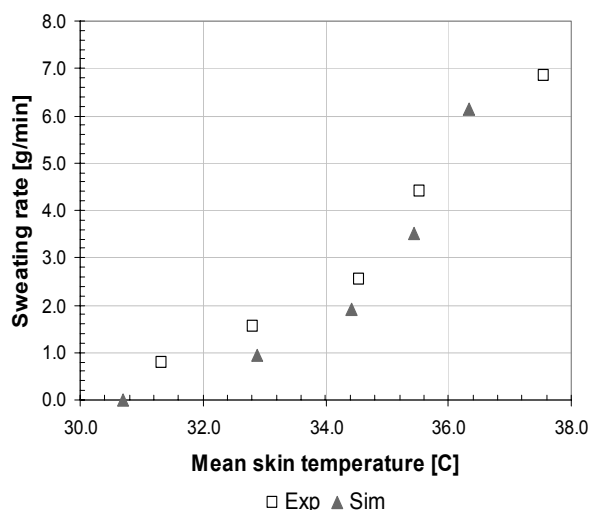

■ Exp 1   ◆ Exp 2   △ Exp 3   + Exp 4   ○ Exp 5   —— Sim.
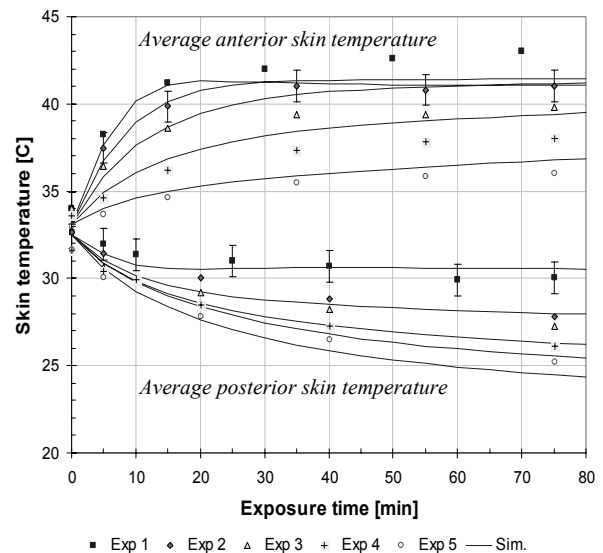
a) Skin temperature

Figure 9. *Comparison of the simulation and experimental results for a human body in asymmetric radiant environments.*
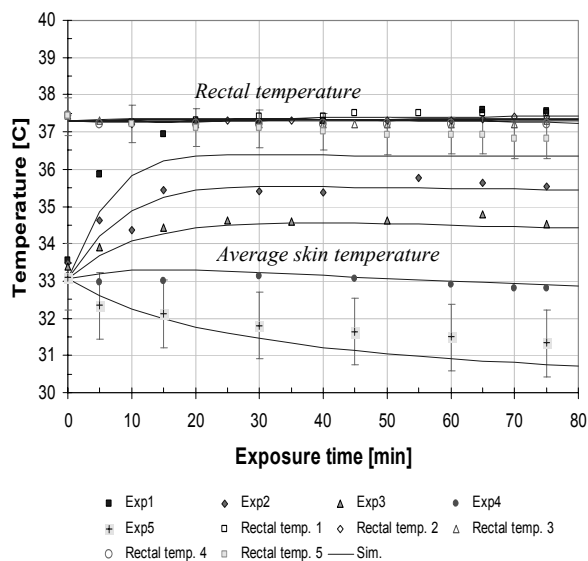
b) Average skin temperature and rectal temperature

c) Sweating rate

Figure 9. (Continued).

The skin temperatures of individual body sectors were predicted and averaged over the anterior and posterior body parts and the whole body according to the experimental protocol. Generally, the simulations agreed well with the experiments for both anterior skin temperatures and posterior skin temperatures (Figure 9a). An exception formed experiment 1, for which the discrepancy between experiment and prediction was greater than the expected experimental error (indicated as bars in Figure 9a). Also the sweating rates and the body core (rectal) temperature predictions were in good agreement with the experimental data (Figure 9b and 9c).

CONCLUSION

The predicted projected area factors and view factors developed here showed good agreement with experimental results obtained by Fanger (1970) and Horikoshi et al. (1996). To illustrate the use of the developed equations the new radiation model was incorporated in an existing multi-segmental dynamic model of human temperature regulation and thermal comfort, Fiala et al. (1999, 2001, 2003). The predictions produced good general agreement with experimental data observed in asymmetric radiant environments.

Scientists and engineer can use the projected area factors and view factors to perform detailed radiation for building occupants. Together with a thermal comfort model these factors will assist architects, designers, building simulation vendors, and researchers to quantify the comfort performance of buildings and HVAC systems, as well as individual built constructions such as windows, heated floor, radiators and etc. The combined model will also have value in analysing the health and safety critical thermal environments.

REFERENCES

CFX-5 (2002). Solver and solver Manager: Radiation in CFX-5, CFX International, AEA Technology plc. Didcot, UK, Release 2002.

Clark J.P. and D. McLean. (1988). ESP – A building and plant energy simulation system. Version 6, release 8, Energy simulation Research Unit, University of Strathclyde and ABACUS Simulations Ltd., Glasgow, UK.

Cook, M. J. and Lomas K. J. (1998). Buoyancy-driven displacement ventilation flows: Evaluation of two eddy viscosity turbulence models for predic-tion. Building Services Engineering Research and Technology, vol. 19, no. 1, pp. 15-21, 1998.

Curran A.R. et al. (1995). Automated radiation modeling for vehicle thermal management, 1995 SAE International Congress and Exposition, Cobo Center, Detroit, USA, March, 1995.

Fanger, P.O. (1970), Thermal Comfort - Analysis and Applications in Environmental Engineering, Technical University of Denmark, Laboratory of Heating and Air Conditioning, McGraw-Hill Book Company

Fiala D., K.J. Lomas and M. Stohrer. (1999). A computer model of human thermoregulation for a wide range of environmental conditions: the passive system. The American Physiological Society, Vol. 87(5), pp. 1957-1972

Fiala D., K.J. Lomas and M. Stohrer (2001). Computer prediction of human thermoregulatory and temperature responses to a wide range of

environmental conditions. International Journal of Biometeorology, Volume 45 (2001), pp 143-159

Fiala D., K.J. Lomas and M. Stohrer (2003). First principles modelling of thermal sensation responses in steady state and transient conditions. ASHRAE Transactions, volume 109, pp. 179-186

Hall J.F. Jr., and F.K. Klemm (1969). Thermal comfort in disparate thermal environments. Journal of Applied Physiology, Vol.27, No.5, pp.601-606.

Horikoshi T. et al. (1996), The effective radiation area and angle factor between man and a rectangular plane near him. ASHRAE Transaction, volume 90, 1996, pp 60-66

Lomas K.J., H. Eppel, C. Martin, and D. Bloomfield. (1994). Empirical validation of thermal building simulation programs using Test Room data. IEA, Energy conservation in buildings and community systems programme. Annex 21: Calculation of energy and environmental performance of buildings and solar heating and cooling programme. Task 12: Building energy analysis and design tools for solar applications: Vol. 1, Final Report, 141-pp., Vol. 2. Empirical Validation Package, 78-pp., Vol. 3, Working Report, 94-pp., 1994.

Poser4. (2000), POSER4, The Premier 3D Character Animation and Figure Design Tool, User Guide for Macintosh and Windows, Curious Labs, Inc.

RadTherm (2001), RadTherm Technical Documentation, Draft, (updated through version 6.0). ThermoAnalytics, Inc.

Stolwijk J.A.J. (1970). Mathematical model of thermoregulation, Physiological and behavioural temperature regulation, chapter 48, Charles C. Thomas Pub., pp. 730-721
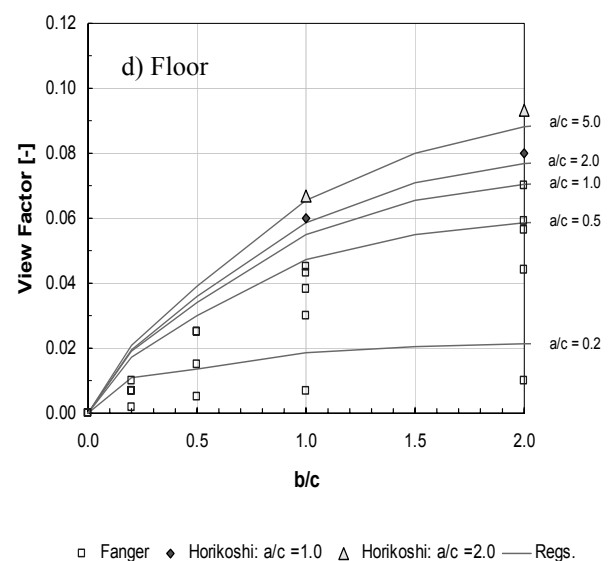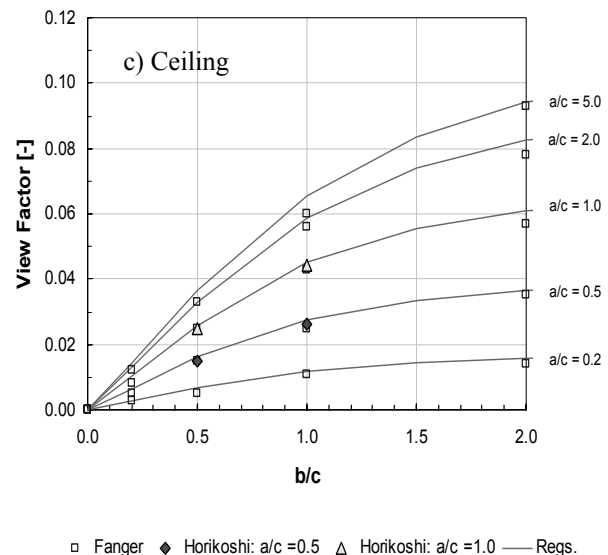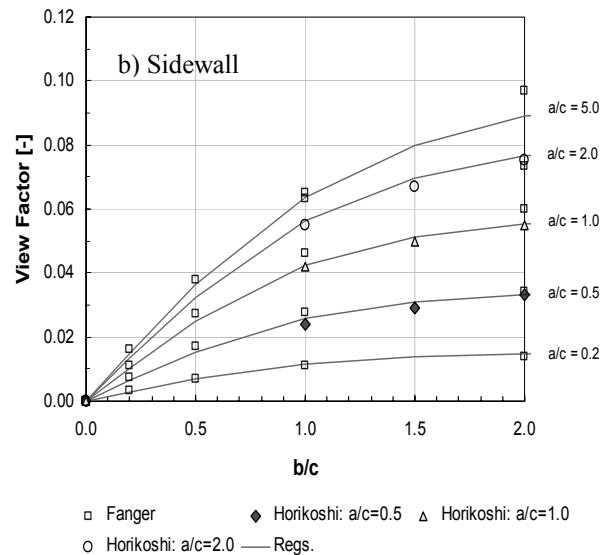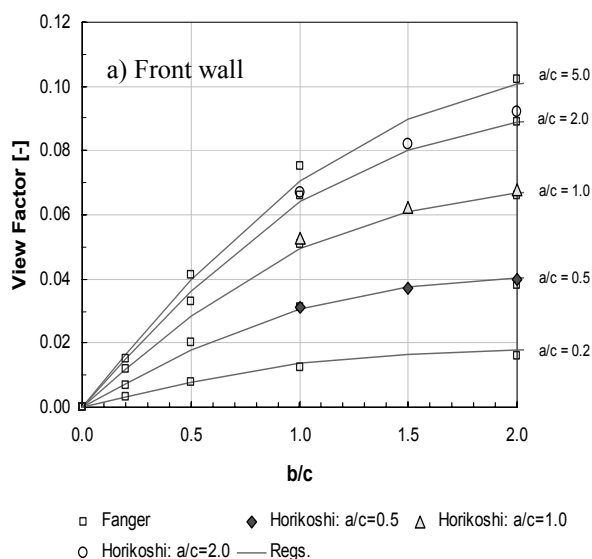
APPENDIX

Figure 10. *Comparison of predicted and measured view factors between a sedentary human body and surrounding planes at different distances.*